Biopolymer Separators from Polydopamine-Functionalized Bacterial Cellulose for Lithium-Sulfur Batteries

Rishav Baranwal[1], Xueyan Lin[1], Wenyue Li[2], Xuan Pan[3], Shu Wang[4], Zhaoyang Fan[2]*

[1]School for Engineering of Matter, Transport & Energy, Arizona State University, Tempe, Arizona, 85281, USA

[2]School of Electrical, Computer and Energy Engineering, Arizona State University, Tempe, AZ 85281, USA

[3]Institutes of Science and Development, Chinese Academy of Sciences, Beijing 100190, China

[4]College of Health Solutions, Arizona State University, Phoenix, AZ 85004, USA

Contact author: zyfan@as.edu

Abstract

The advancement of the lithium-sulfur (Li-S) batteries is immensely impeded by two main challenges: polysulfide shuttling between the electrodes and Li dendrite formation associated with the Li-metal anode. To tackle these challenges, we synthesized a polydopamine coated bacterial cellulose **(**PDA@BC) separator in a way to create physical and chemical traps for the shuttling polysulfides and to control the Li^+ flux. While nanocellulose offers its dense network as a physical trap, the presence of polydopamine in the separator offers polar functional groups which not only has a high binding energy towards the polysulfides but also helps in redistribution of the Li^+ ions across it. The electrochemical and physiochemical results suggest that the synthesized separator can have practical applicability owing to its superior performance compared to a commercial separator. The Li-S batteries assembled with this separator showed a specific discharge capacity of 1449 mAh g^{-1} at 0.1C and 877 mAh g^{-1} at 1C, and a capacity fade of 0.03% per cycle over 650 cycles at 1C. Using a PDA@BC separator, a practical Li-S battery cell with S loading of 7.5 mg cm^{-2} (and E/S ratio of 10 µLmg^{-1}, 82% S ratio) was also tested at 1C, which delivered a capacity of ~ 6 mAh cm^{-2} for 500 cycles.

Keywords: Battery separator, Polydopamine, Bacterial cellulose, Lithium sulfur battery, Li-metal battery

1. Introduction

Demands for electrified transportation and renewable energy require high-performance electrical energy storage devices. Lithium-ion batteries are currently playing a dominant role among these devices, but with limitations on cost, material availability, and low capacity. Towards next-generation battery technology, a strong interest exists in developing Li-S batteries. A high theoretical capacity of 1675 mAh g^{-1} for sulfur, along with its earth abundance and low cost, justifies the effort in developing this battery technology [1].

Besides the notorious dendrite challenge associated with the Li-metal anode, Li-S chemistry also suffers from a lithium polysulfide (LiPS) shuttling problem. With a cyclic ring (cyclo-octasulfur) structure, sulfur in the cathode undergoes stepwise reduction during discharge, forming long-chain and short-chain polysulfides. The long-chain LiPS (Li_2S_x,$4 \leq x \leq 8$) can easily dissolve in the used ether-based electrolyte and diffuses out of the cathode matrix to the anode side, where it reduces and then transports back to the cathode. The resulting polysulfide shuttle effect leads to low Coulombic efficiency, anode corrosion, rapid capacity decay, and fast battery failure, sabotaging the practical utilization of Li-S battery technology[2, 3]. To address this problem, studies mainly focus on the cathode material and structure design to physically trap and chemically bind these soluble polysulfide species into a porous cathode matrix [2, 4, 5]. In particular, various catalysts, such as transition metal compounds[6-11], atomically distributed metals [12-15], and others[16-18], are actively investigated to catalytically accelerate the multistep and liquid/solid phase redox conversions, thus minimizing the LiPS shuttling. Other methods such as adopting electrolyte additives[19], inserting a blocking interlayer between the cathode and the separator[20-23], and functionalizing the battery separator[24], have also been reported.

The primary function of the separator in a Li-based battery is to electrically isolate the active cathode and anode materials but allow free transportation of Li^+ ions. A separator allowing active LiPS shuttling between two electrodes does not fulfill its essential function. Therefore, modifying the separator to shut off LiPS shuttling is a straightforward and attractive strategy. Blocking the LiPS pathway can be achieved via pore size downscaling to a few nanometers that allow Li^+ transportation but not LiPS[25]. Another attractive

method is to graft polar functional groups on the separator [26-29]. Strong intermolecular forces can be established between these functional groups and LiPS, confining them to the cathode side[25, 30-32].

A functional separator can also positively impact the Li-metal anode performance. With reduced LiPS shuttling, the adverse effect of LiPS on the Li-metal surface is addressed. More importantly, by engineering a separator with a uniform nanoscale pore distribution and functional chemical group distribution, the Li^+ flux at the anode surface will be much more consistent and uniform than when a commercial separator is used[29, 33-35]. The implementation of such a separator would provide a partial solution to the complex issue of Li dendrite formation. This problem is closely associated with the local high density of Li^+ flux, which is partly attributed to its nonuniform flux at the anode.

Commercial battery separators are extruded polyolefin films, which cannot address the challenges of LiPS shuttling and Li-metal dendrite formation. Natural polymers and cellulose have gained traction in developing multifunctional separators for Li-S[36-38] and other battery technology[39-44]. This is particularly true for bacteria cellulose (BC), which is superior to plant-derived celluloses because its higher purity and better crystallinity vest it with much better mechanical, thermal, and chemical properties[45].

Polydopamine (PDA) is another exciting biopolymer. With phenolic hydroxyl, ortho-quinone, amine, and imine functional groups[46, 47], PDA can strongly bind with many molecules, including LiPS[48]. Herein, we report a biopolymer separator for Li-S and other Li-metal batteries based on polydopamine-functionalized bacteria cellulose membrane. With BC submerged in a mild solution, dopamine is oxidized and polymerized to form a thin PDA coating on the BC nanofibers. The resulting lithophilic PDA@BC membrane with a uniform pore distribution can strongly bind LiPS and regulate Li^+ transportation, thus helping address the two challenging problems of LiPS shuttling and Li dendrite formation in Li-S chemistry. Our physicochemical and electrochemical studies revealed the excellence of PDA@BC as a separator for Li-S batteries. Li-S cells using the PDA@BC separator demonstrate dramatically improved performance with a specific capacity of 1449 mAh g^{-1} at 0.1C and 877 mAh g^{-1} at 1C.

2. Experiments

2.1 Materials

Tris-HCl (99%), 1,3-dioxolane (DOL) (99%), dimethyl ether (DME) (99%), lithium bis(trifluoromethanesulfonly)imide (LiTFSi) (99.95%) and lithium nitrate ($LiNO_3$) (99.99%) were purchased from Sigma Aldrich. Lithium sulfide (99.9%) (Li_2S) was purchased from Fischer Scientific.

2.2 Synthesis of polydopamine-functionalized bacterial cellulose (PDA@BC) separators

30 g of BC sheet was impelled in 100 mL of DI water to form dispersed BC nanofiber suspension (Fig. S1 in the Supplementary Information (SI)). Polydopamine hydrochloride (2 gL^{-1}) and 10 mM tris-HCl solution (pH=8) [49, 50] were used for functionalizing the BC. It was added to the cellulose solution under vigorous stirring and left for 24 hours in the air under a fume hood for PDA polymerization. The white color of the solution turned brownish-black due to the PDA coating on the BC. This solution was used to make a membrane via the vacuum filtration method. The formed film was washed with DI water to remove any unreacted precursors. After this step, solvent exchange with ethanol removed water from the membrane. It was peeled carefully from the filter paper and kept between two glass slides for vacuum drying at 120°C for 12 hours. The separator was roller pressed at 80°C to reach a thickness of 30 μm.

2.3 Separator Characterization

Differential scanning calorimetry (DSC) was performed for the BC-based and the commercial Celgard 2400 (C-2400) separators to study their thermal stability. Scanning electron microscopy (SEM) was performed to characterize the sample's morphology. The chemical bonding information was revealed using Fourier transform infrared spectroscopy (FT-IR). Further, the composition and chemical bonding information of the separator was studied using an X-ray photoelectron spectroscope (XPS).

For evaluating Li^+ ion conductivity through the separator, the PDA@BC separator was soaked in the electrolyte (1M LiTFSI in 1:1 DOL: DME vol. ratio, with 1 wt% $LiNO_3$ as the standard electrolyte used in this work) and then sandwiched between two stainless steel spacers inside a coin cell. Electrochemical impedance spectroscopy (EIS) was conducted on a Bio-logic workstation to measure the bulk resistance. Li^+ ion conductivity was calculated using the equation $\sigma = L/RA$, where L is the thickness of the

separator, R is the measured bulk resistance, and A is the electrode area. Li-Li symmetric coin cells (CR2032) were assembled with PDA@BC or C-2400 as the separator to measure their transference number, $t = I_s(V-I_oR_o)/I_o(V-I_sR_s)$, where I_o and I_s are the initial and steady-state current obtained after 1000 s, V is the applied potential, R_o and R_s are the resistance before and after DC polarization.

2.4. Battery assembly and electrochemical study

Freestanding sulfur cathodes were used. BC sheets were first hydrolyzed in DI water at 80°C for 2 days until the sheets were fully saturated. These sheets were freeze-dried at -85°C and 0.72 mm Hg to remove the water, which were further carbonized at 800°C in an argon environment for 2 hours. Discs with a diameter of 10 mm were punched from these carbonized sheets onto which 0.25 M Li_2S_6 catholyte was added to form the freestanding sulfur cathodes during assembly.

Li-S coin cells (CR2032) were assembled using the freestanding cathodes, PDA@BC or C-2400 as the separator, Li chips as the anode, and the above standard electrolyte. These cells were created with different sulfur loadings of 5 mg cm^{-2} and 7.5 mg cm^{-2} and their corresponding E/S ratios of 15 and 10 µL mg^{-1}. The galvanostatic charge/discharge was performed between 1.7-2.8 V at different current rates. Cyclic Voltammetry (CV, scan rate: 0.1-0.4 mV/s, voltage range: 1.7-2.8 V) and EIS (0.1 Hz-100 kHz with 10 mV AC voltage amplitude) were conducted on a Bio-logic workstation. Li-Li and Li-Cu cells were assembled to study the impact of the separator on the Li plating-stripping behavior. All cells were tested and recorded in a LANHE battery testing machine.

3. Results and Discussion

3.1. Polydopamine coated bacterial cellulose material properties.

The coating of PDA on BC fibers can be understood through the schematic in Fig. 1a. Dopamine has an amine group (-NH), which undergoes oxidation in an alkaline environment to yield unstable intermediates, as schematically shown in Fig. S2 in the SI. As a result, the structure undergoes cyclic rearrangement, which causes the creation of multiple nucleophilic structures with aromatic nitrogen groups[51]. The delocalized electron density on these unstable intermediates drives the nucleophilic

attachment of these oxidized dopamine molecules to the cellulose. To bind with cellulose, these intermediaries go through the Michael Addition and Schiff Base reactions. In addition, the oxidized dopamine self-polymerizes by joining and cross-linking with one another [52]. The binding between PDA and BC is also accelerated by the dehydration between catechol of PDA and hydroxyl groups of BC[49]. The presence of amino and phenolic groups in these molecules leads to enhanced binding among them through hydrogen bonding. Fig. S3 in SI reveals the formation of stable PDA coated BC nanofibers. XPS analysis of the composite reveals the presence of N and O groups suggesting PDA coating on BC (Fig. S4 in SI).

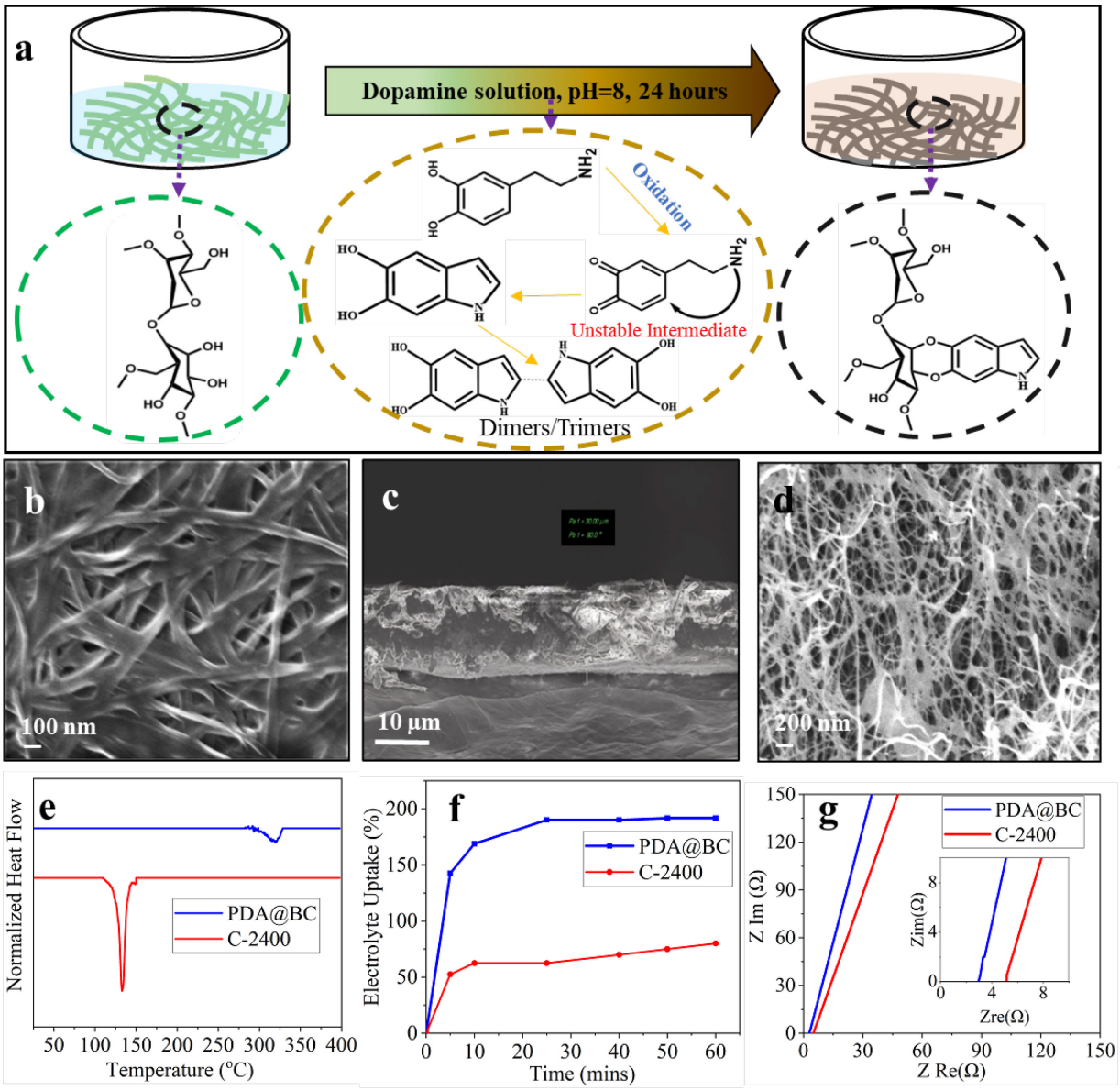

Figure 1. a) Schematic of PDA coating on BC. SEM Images of PDA@BC **(b** and **c)** and carbonized BC **(d)**. **e)** DSC curves, **f)** electrolyte uptake capability, and **g)** ion conductivity test for PDA@BC and C-2400 separators.

The formed PDA@BC separator was observed under SEM to reveal their surface morphology. Fig. 1b and Fig. S5 in the SI show that the PDA coated cellulose nanofibers are cross-linked with each other forming an interconnected network with distributed nanopores. Such a morphology can facilitate the transportation of the Li^+ ions with a uniform flux [53]. PDA@BC contains various functional groups, shown

in the FTIR spectra (Fig. S6 in the SI). The presence of the N and O groups, being part of the indole/indoline type derived structures from PDA, are shown by the intensity spectra between ~1500 and 1700 cm^{-1}[54]. The intensity peak around ~1210 cm^{-1} corresponds to the C-O stretching formed by dehydration of catechols and hydroxyl groups, while peaks around ~900 and 800 cm^{-1} refer to the C-H and C=C stretching from BC and PDA[3, 49]. The spectra show a weak peak at ~3400 cm^{-1} of -OH groups, suggesting that most hydroxyl groups were dehydrated to C-O bonds[55].These results confirm the coating of PDA on BC via dehydration, imine interaction, and hydrogen bonding. The cross-sectional SEM image (Fig. 1c) confirms the formation of a 30 μm thick, porous separator. Fig. 1d shows the SEM images of a free-standing carbonized scaffold derived from BC as the sulfur host. The spaced-out networks as seen in the image, provide mesoporous and microporous spaces for S loading[56]. This interconnected carbon nanofiber scaffold facilitates high sulfur loading in the cell with ionically and electronically conductive pathways for the ionically and electronically highly insulating sulfur and Li_2S. Raman Spectra of carbonized BC (Fig. S7 in the SI) shows the defective and disordered structure represented by D band at 1350 cm^{-1} and the crystalline graphitic carbon represented by G band at 1580 cm^{-1} ($I_D/I_G = 1$). The presence of these defects increases accessible pore volume to trap LiPS.

A porous separator should provide excellent isolation between the anode and cathode even at high temperatures to prevent thermal runaway. As is known, the C-2400 separator will be molten at elevated operation temperatures (>~100 ºC), causing catastrophic battery failure. Separators with much-improved temperature tolerance features will enhance battery safety. We tested the thermal stability of our PDA@BC membrane in an oven along with the C-2400 from room temperature to 140°C. The PDA@BC membrane, as shown in Fig. S8, retained its shape without any signs of deformation while the commercial separator decomposed. Indeed, DSC measurements in Fig. 1e show that C-2400 has an endothermic decomposition peak around 140ºC, while it is about 340°C for our PDA@BC, suggesting the PDA@BC with much better temperature tolerance. The high crystallinity of BC renders its intrinsic thermal stability, while the closed-packed chains of polysaccharides in PDA@BC, due to their hydrogen bonding, further contribute to this property [49, 52, 57]. Hence, using PDA@BC as a separator can ensure safe battery operation at higher

temperatures. The biopolymer separator was also folded multiple times, after which its original shape was regained, showing the excellent flexibility of the prepared PDA@BC membrane (Fig. S9 in the SI).

This porous separator should also be able to hold a specific volume of electrolyte to ensure facile transport of Li^+ across the separator with a substantially small internal resistance in the battery. To measure their electrolyte uptake capabilities, separators were submerged in the DOL-DME-based electrolyte, and the mass change over an hour was recorded. Fig. 1f demonstrates the superior electrolyte uptake capabilities of PDA@BC, with an initial accelerated absorption of up to 150%. We further measured the contact angle to show the wetting nature of the separators. As shown in Fig. S10 in the SI, C-2400 has a contact angle of 26.5° after the initial resting time, as opposed to 0° of the PDA@BC separator. The presence of N- and O-abundant sites in PDA@BC increases its surface energy due to which they have a strong affinity towards the used electrolyte, and hence the electrolyte gets thoroughly soaked in it showing better wettability [58].

Cells were assembled with two stainless steel spacers as electrodes, a separator, and an electrolyte to determine Li^+ ion conductivity across the separator. We conducted EIS measurements, and the Nyquist plot for both separators is shown in Fig. 1g. The ionic conductivity across the separator was calculated to be 0.37 mS cm^{-1} for PDA@BC, compared to 0.21 mS cm^{-1} for C-2400. These excellent electrical characteristics of PDA@BC can be accredited to its multiple functional groups and lithophilic nature that offer facile diffusion pathways for Li^+ [59]. PDA contains functional groups like amine and phenolic hydroxyl groups, and these groups exhibit an affinity for Li-ions[60]. But this affinity is not strong so that Li-ions attached to these sites can be transferred through the conjugated π electrons in chains of PDA [61] as shown in Fig. S11. There is charge transfer interaction between the benzoquinone groups of one chain to the catechol groups of other chain [62], which also allows transportation of Li+ ions through the biopolymer as well. To measure the Li^+ transference number, DC potential of 10 mV was applied to the cell, and their current response was recorded for the specified time. The chronoamperometry and EIS graphs are shown in Fig. S12 and S13 in the SI, and the related parameters are listed in Table S1. The transference number for PDA@BC is ~0.74 compared to 0.65 for C-2400, suggesting that the former facilitates Li^+ transportation. The porous structures of PDA@BC, along with its lithiophilic features, offer highly diffusive

pathways enabling faster transportation of these charged ions. These results suggest that PDA@BC offers ameliorated separator characteristics compared to the C-2400.

3.2. Cyclic voltammetry and electrochemical impedance spectroscopy studies

CV study of Li-S cells, in the potential window of 1.7-2.8 V, was conducted further to elucidate the improved functionality by the PDA@BC separator. Fig. S14a in SI compares the CV curves for both separators at a scan rate of 0.1 mV s^{-1}. The curves show reduction of S to Li_2S_x (x>=4) and succeed to Li_2S/Li_2S_2 occurring at potentials of 2.3 V and 1.98 V for PDA@BC, compared to 2.27 V and 1.95 V for C-2400. The CV curves of Li-S batteries at increasing scan rates from 0.1 to 0.4 mV s^{-1} with PDA@BC (Fig. S14b) shows a more positive and negative shift in the anodic and cathodic peaks respectively compared to C-2400 (Fig. S14c), hinting an improved reaction kinetics for Li-S cell [63] with PDA@BC as the separator. The polarization values at each scan rate are listed in Table S2 in the SI. For the redox peaks, the peak current density I_p and square root of scan rate $v^{1/2}$ was linearly fitted using the equation $I_P = 2.69 \times 10^5 n^{3/2} A D^{1/2} v^{1/2} C$, where n, A, and C represent the charge transfer number, the active electrode geometric area, and the concentration of Li^+, respectively. As shown in Fig. S14d, the larger slope for the PDA@BC cell indicates faster rate of Li^+ ion diffusion with the biopolymer membrane [64].

EIS measurements were done on freshly assembled Li-S coin cells to reveal the charge transfer resistance (R_{ct}). Fig. S15a shows the Nyquist plot of the EIS spectra. The functional groups of N and O in the membrane creates active sites on the separator allowing redistribution of the Li^+ ions, and a uniform flux of Li^+ ions facilitates a lower resistance and higher diffusion [65]. These cells were subjected to EIS measurements again after CV cycling to investigate any change in the electrochemical processes inside the Li-S cells. The results are shown in Fig. S15b for PDA@BC and C-2400, respectively. These cells show a resistive element due to the diffusion of ions across the SEI formed during the cell activation [66]. The reduction in R_{ct} values post CV can be explained by increased activation sites, improved electrolyte availability in the cathode, and increased diffusion pathways [67].

3.3. Lithium stripping and plating in Li/Li and Li/Cu cells

The separator in a battery controls the Li^+ flux distribution at the microscale, and this flux distribution impacts the Li deposition and stripping. The unstable stripping of the Li^+ ions from the anode side during discharge leads to the formation of whiskers and pits [68], deteriorating its long-time performance. The formation of these irregularities can be studied by their corresponding overpotentials in a Li-Li symmetric and Li-Cu asymmetric cell.

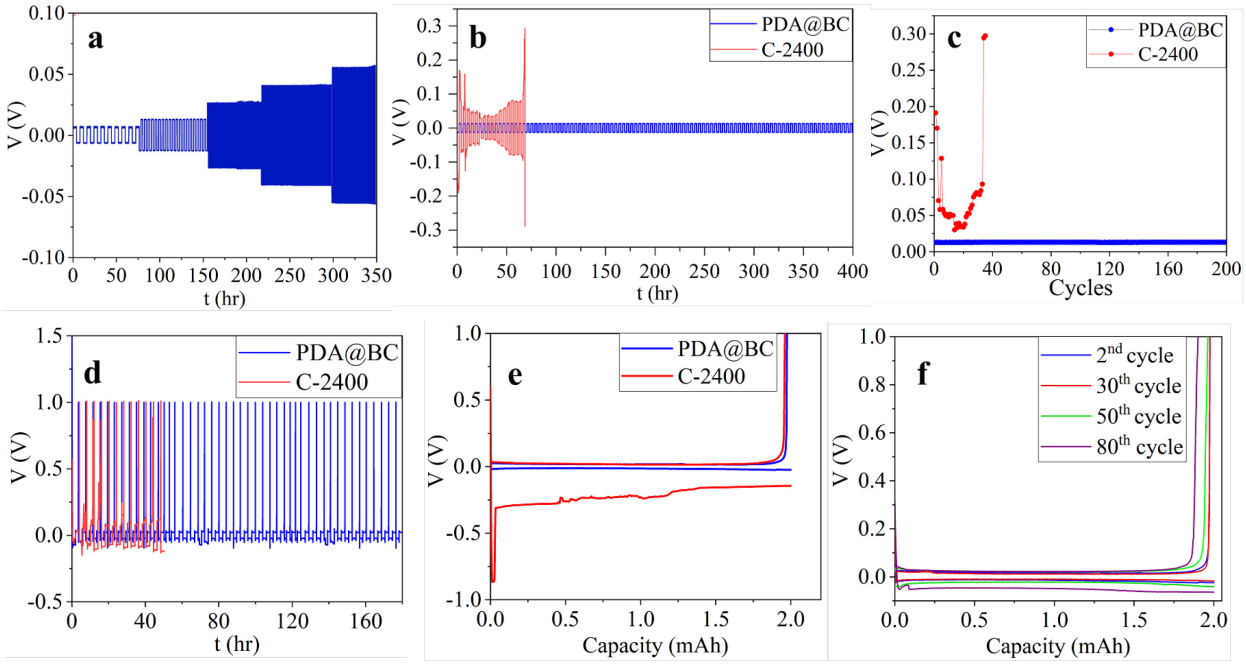

Figure 2. Li-Li plating-stripping study of **a)** PDA@BC from 0.5 to 6 $mAcm^{-2}$, **b)** PDA@BC and C-2400 at 1 $mAcm^{-2}$. **c)** Overpotentials measured from b). Lithium plating-stripping result of Li-Cu unsymmetric cell with **d)** PDA@BC and C-2400 separators at 2$mAhcm^{-2}$ discharge capacity and their second cycle Voltage-capacity graph **(e). f)** Li-Cu plating stripping with PDA@BC separator showing voltage-capacity curves at different cycles.

Galvanostatic cycling tests of Li-Li cells were carried out. Fig. 2a shows the plating-stripping behavior of the PDA@BC cell under a constant capacity of 2 mAh cm^{-2} but at different currents, with overpotentials of 7, 13, 27, 41 and 55 mV for a current of 0.5, 1, 2,4 and 6 mA cm^{-2}, respectively. Fig. 2b compares the long plating-stripping behavior of PDA@BC and C-2400 at a current of 1 mA cm^{-2} and a capacity of 1 $mAhcm^{-2}$. For the C-2400 cell, the potential flickered in each cycle, and the cell quickly reached a cutoff potential of 300 mV after just 70 hours of cycling test. These observations suggest C-2400 failed to maintain a stable Li plating and stripping process by curbing dendritic growth. PDA@BC, in comparison, shows more than 400 hours of stable cycling with an almost invariable overpotential of 13 mV. Fig. 2c maps the overpotentials measured in case of both stripping and plating behavior, from Fig. 2b, for each cycle. The symmetric cells with C-2400 reports variable overpotentials in almost every cycle with a minimum overpotential of 30 mV, clearly indicating the presence of irregular Li flux across it. The magnified voltage time profiles at different cycles, shown in Fig. S16-17, confirm the same. We hypothesize that the nitrogen based functional group present in the biopolymer membrane facilitates chemical interactions with the Li ions [69] due to the delocalized electron density in the indole groups. These uniformly distributed functional groups homogenize the Li ions across the membrane giving rise to stable and symmetric plating-stripping.

Li-Cu cells were also assembled to test the Li stripping and plating behavior under the two separators. Lithium was plated on the copper electrode first at a constant discharge capacity of 2 mAh cm^{-2}, and it was then plated back while maintaining a cutoff voltage of 1 V. Fig. 2d compares the plating-stripping in these cells at 1 $mAcm^{-2}$. The cell with C-2400 separator has a cyclic capability of ~50 hours with unstable stripping and plating behaviors leading to dendritic growth and, ultimately, membrane penetration leading to its failure. Li-Cu cells with PDA@BC separator have a cyclic capacity of more than 180 hours. Voltage-capacity curves for their second cycles are presented in Fig. 2e. Uniform removal and deposition of lithium occurs at a lower overpotential, 19 mV, for the functionalized separator, whereas the C-2400 shows not only non-uniform stripping and deposition characteristics but also higher polarization potentials suggesting its inability to protect anode at higher discharge rates. To further demonstrate the effectiveness of using this

biopolymer-based separator, the voltage-capacity profiles for its different cycles are shown for the Li-Cu batteries assembled with PDA@BC separator in Fig. 2f, where there is an almost negligible increase in the overpotentials. The coulombic efficiency derived from the Li-Cu study has a value of 98.9% after 80 cycles, while there is quick fade observed for C-2400 (Fig. S18). The chemical interactions between the functional groups and the Li ions help in its redistribution in the initial few hours of the first cycle of plating, leading to its uniform deposition on the copper foil. These studies justify the use of PDA@BC addressing the dendritic issues in the lithium-metal cells.

3.4. Polysulfides adsorption test

To meet the basic design requirements for a separator in a Li-S battery, waning the polysulfide (PS) shuttling is a pivotal design consideration as it leads to continuous capacity degradation. Hence, PDA@BC and C-2400 separators were tested for their adsorption ability towards LiPS by dipping in 0.1 mM Li_2S_6 solution. The chemical interaction of the LiPS with PDA@BC separator can be physically observed in Fig. 3a. The yellow color of the LiPS solution slowly faded away, in the vial with PDA@BC, to an almost clear solution suggesting the adsorption of the LiPS from the solution, while the vial with C-2400 separator retained the same color. The chemical configuration and interaction between the PDA@BC separator and polysulfides were studied by X-ray photoelectron spectroscopy (XPS) before and after polysulfide adsorption tests. In the wide XPS surveys (Fig. 3b), new peaks appeared at 57.1 eV and 168.7 eV corresponded to the Li 1s and S 2p regions after polysulfide adsorption. In the high-resolution S 2p spectrum (Fig. 3e), two nearby peaks at 161.8 eV and 163.3 eV correspond to terminal S and bridging S, respectively, which indicates effective polysulfides trapping by the separator [70]. The peaks at 168.3 and 166.4 eV correspond to polythionate and thiosulfate, respectively[70]. In the Li 1s spectrum (Fig. 3f), the peak at 54.6 eV [71]corresponds to the Li–S bond of polysulfides, and the peak at 57.2 eV corresponds to newly formed Li–O and Li–N[72] bonds between polysulfides and O, N-containing groups of the separator, which served as lithophilic sites to form Li–O and Li–N bonds with polysulfides. This demonstration is further validated by the presence of Li–O bonds (530.9 eV) in the O 1s spectrum (Fig. 3g) and Li–N bonds (401.9 eV) in the

N 1s spectrum(Fig. 3g) [73]. Thus, polysulfides were found to be chemically trapped by the PDA@BC separator by forming Li–O and Li–N bonds. This confirms our hypothesis that these functional groups not only block the PS but also regulate the Li ion flow by forming these chemical bonds. A schematic of the interaction between these groups is shown in Fig. 3i. The LiPS solutions after 48 hours of adsorption with the separators were analyzed with UV spectroscopy. The concentration of the LiPS as seen in the absorbance spectra in Fig. S19 is significantly higher in the solution obtained with C-2400 compared to PDA@BC. This suggests that more polysulfides have been attached to the lithiophilic sites on the PDA@BC separator. The PS diffusion test was also conducted in an H-cell setup with PS solution in one arm and blank solution in the other, with the separator in between as shown in Fig. S20. Over the span of 48 hours, PDA@BC absorbs the polysulfides present in the solution rendering it transparent, while C-2400 shows the apparent diffusion of the PS. Hence, integrating the results of these experiments, we zero in on the conclusion that the PDA@BC can effectively inhibit the PS shuttling.

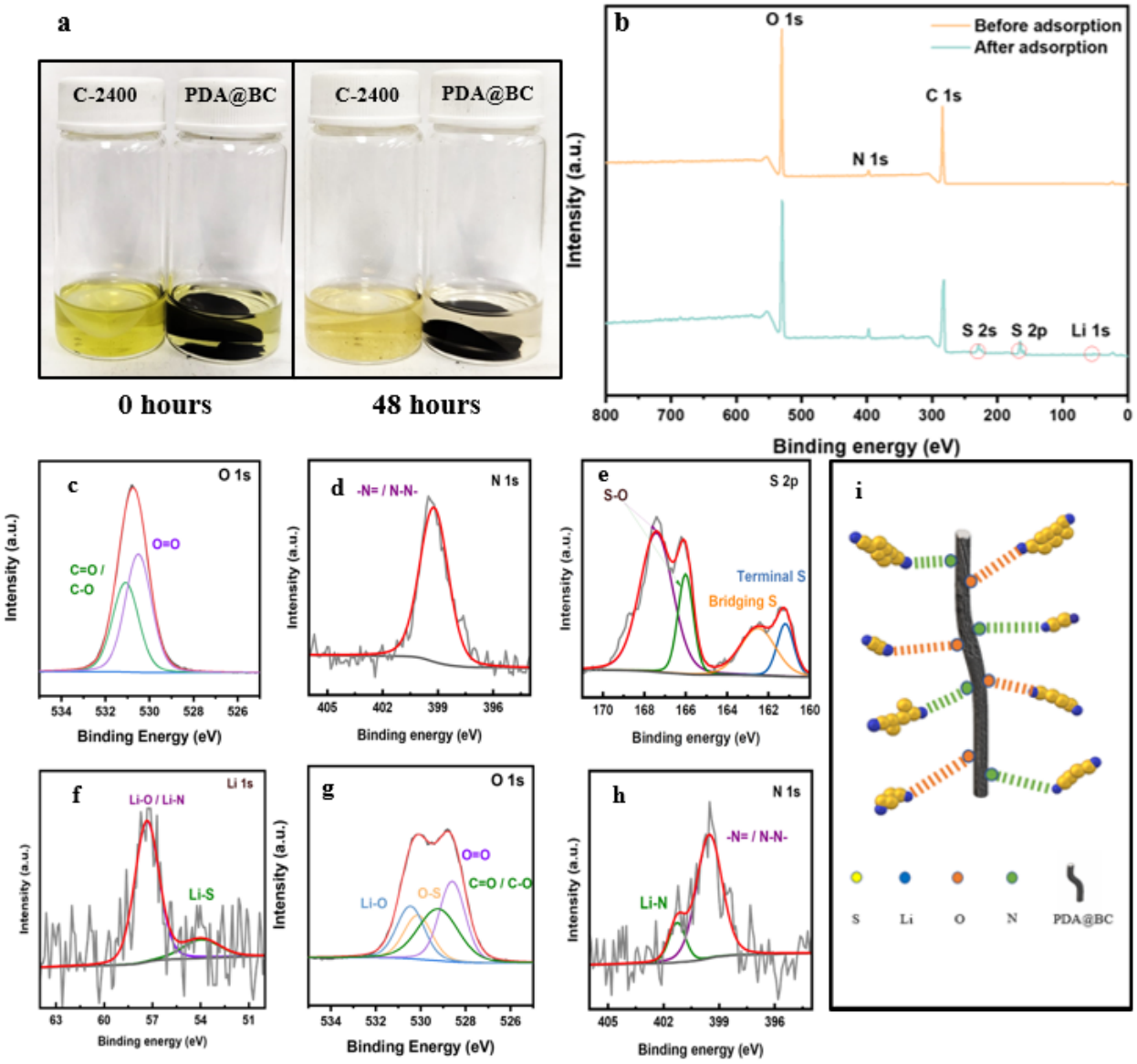

Figure 3. a) Optical photographs of LiPS solution in PDA@BC and C-2400 Separators. **b)** XPS survey spectra of the PDA@BC separator before and after PS adsorption. **c)** N 1s and **d)** O 1s spectra of PDA@BC before XPS adsorption**. e)** O 1s, **f)** N 1s, **g)** S 2p and **h)** Li 1s spectra obtained from PDA@BC after PS adsorption. **i)** Schematic representation of the PS trapping by a fiber of PDA@BC.

3.5. Lithium-sulfur battery cell performance

Li-S coin cells were assembled with PDA@BC and C-2400 separators to conduct various electrochemical studies. After the first discharge and charge cycle, the cell underwent an open circuit potential (V_{OC}) test. Under this condition, the decay of V_{OC}, corresponding to capacity loss, is fueled by various self-discharge mechanisms, of which LiPS shuttling is perhaps the most significant one in a Li-S cell [74]. Fig. 4a shows a dramatic voltage loss of ~ 60 mV for a typical C-2400 cell in 12 hours, while almost no loss in the potential was observed for a PDA@BC cell. This suggests that under the no load condition, the LiPS shuttling has largely been curbed by the PDA@BC biopolymer separator.

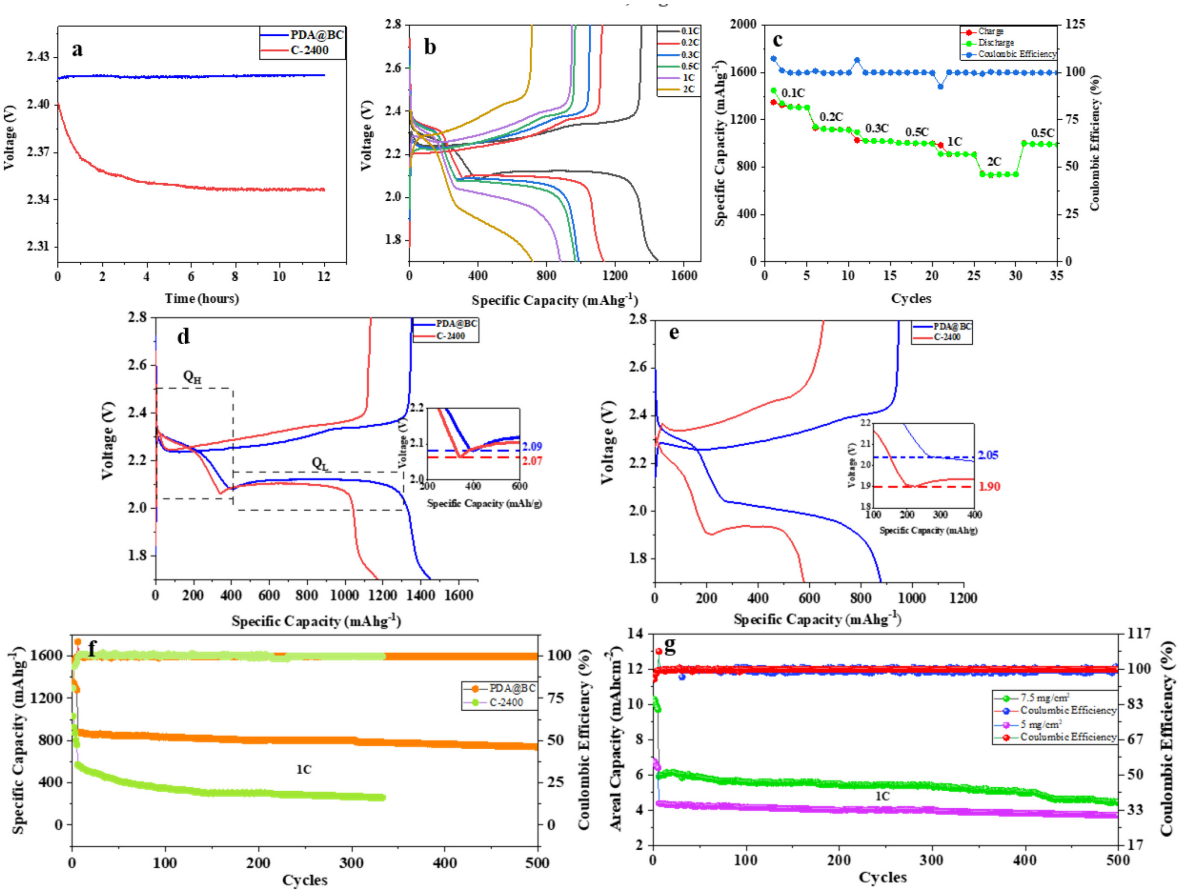

Figure 4. a) Open circuit potential test of Li-S battery with PDA@BC and C-2400 separator. **b)** Voltage profile and, **c)** Rate capability of Li-S Battery with PDA@BC at different current densities. Voltage profiles of Li-S Batteries with PDA@BC and C-2400 at **d)** 0.1 and **e)**1C. **f)** Cyclic performance of Li-S with PDA@BC and C-2400 at 5 $mgcm^{-2}$ S loading and **g)** Areal capacity of the Li-S cells with PDA@BC as a separator and having sulfur loadings of 5 and 7.5 $mgcm^{-2}$, respectively.

The impact of this new separator on cell rate performance was further investigated. The assembled Li-S cells were charged and discharged at different rates from 0.1 to 2 C and then back to 0.5C. The cell showed a first cycle capacity of 1449 mAh g^{-1} at 0.1C, which reduces to 877 mAh g^{-1} at 1C (Fig. 4b). We observe that the separator allows capacity reversibility in the Li-S battery as it regains its capacity after running at higher discharge rates (Fig. 4c). In contrast to this, the Li-S battery with C-2400 shows an initial capacity of 1171 mAh g^{-1} at 0.1C while having a significantly reduced capacity of ~600 mAh g^{-1} at 1C (Fig. S21). The charge-discharge profiles of Li-S battery with PDA@BC and C-2400 at 0.1 and 1C are shown in Fig. 4d and e, respectively. There are two capacity-determining steps in a Li-S battery during discharge, which are represented by Q_H in Fig. 4d, referring to the higher capacity step in which sulfur reduces to long chain soluble PS, and Q_L, the lower capacity step in which the long chain PS further reduce to insoluble short chain PS [66]. Shuttling of these soluble PS is effectively suppressed with the use of PDA@BC, as indicated by higher values of Q_H and Q_L. The reduction of sulfur/polysulfides in these steps also occurs at a lower potential for C-2400 compared to PDA@BC (~2.09V vs. 2.07V at 0.1C), and it reduces drastically at a higher discharge rate for C-2400 (~1.9V at 1C). The disappearance of the discharge reduction peak at a high discharge rate of 2C in the case of C-2400 suggests irreversible battery degradation. Hence, to compare the performance of Li-S batteries with these separators at a high discharge rate, these cells were cycled at 1C at 5 mg cm^{-2}, 75% S loading, with the first five cycles at 0.1C. Fig. 4f clearly justifies the use of PDA@BC separator in Li-S battery against the commercially available one. It offers a specific capacity of over 879 mAh g^{-1} in the first cycle while fading to 707 mAh g^{-1} after 650 cycles of runtime with an average fade of 0.27 $mAhg^{-1}$ each cycle, while the latter has an initial specific capacity 592 mAh g^{-1} while fading to ~300 mAh g^{-1} in 130 cycles and maintaining that over the next 200 cycles before its complete failure. The Coulombic efficiency observed is very volatile in the case of C-2400, hinting at unstable electrode reactions due to irregular diffusion of Li ions, while it is almost constant and always >~98.5% with slight fluctuations for the biopolymer separator. The Li-S battery with PDA@BC was also tested at 1C with S loading of 7.5 mg cm^{-2} (and E/S ratio of 10 µL mg^{-1}, 82% S loading) to check for its cyclic

performance under high loading conditions. Fig. S22 shows Li-S battery has an initial capacity of 747 mAh g^{-1} while reaching a maximum specific discharge capacity of 776 mAh g^{-1}, maintaining a capacity of 630 mAh g^{-1} after 400 cycles and fading to 498 mAh g^{-1} in the next 150 cycles. The areal capacity at 1 C for these S loadings is plotted in Fig. 4g, showing excellent capacity retention, having a first cycle capacity of 6.39 $mAhcm^{-2}$ and 3.7 $mAhcm^{-2}$ respectively.

3.6. Postmortem studies of the lithium anode and the polydopamine functionalized bacterial cellulose separator.

The evolution of dendrites, pits, and other surface irregularities over the long cyclic performance will suggest irregular stripping and plating from the Li anode caused by repeated SEI breakage due to polysulfide corrosion. Hence, the Li-S cells with both these separators were disassembled after certain cycles to observe the Li evolution and redeposition under SEM. The Li chips of Li-S cell with C-2400 after 100 and 200 cycles are shown in Fig. 5 a1-a2 and b1-b2 at two different magnifications, respectively. The change in morphology from a planar structure (Fig. S23) to grainy coarse deposits in the first 100 cycles to highly irregular deposits, forming pits and extrusions on the surface in the next 100 cycles can be observed. The Li surface from the Li-S cell with PDA@BC separator shows (Fig. 5 c1-c2) compact deposits on the surface. These deposits undergo moderate surface degradation while remaining compact and uniform after 500 cycles as seen in Fig.5 d1-d2. Fig. 5 a2 and c2 compare Li deposits for C-2400 and PDA@BC after 100 cycles. The difference in the morphology of the deposits can be attributed to the controlled growth of the Li facilitated by PDA@BC. The evolution of small uneven agglomerates from larger agglomerates suggests the dendritic growth for C-2400 (Fig. 5 b2) which would lead to formation of dead Li and much worse the cell failure eventually, while Fig. 5 d2 shows continued compact deposits reverberating the reversible nature of the plating-stripping and the protection of the Li anode from corrosive polysulfides.

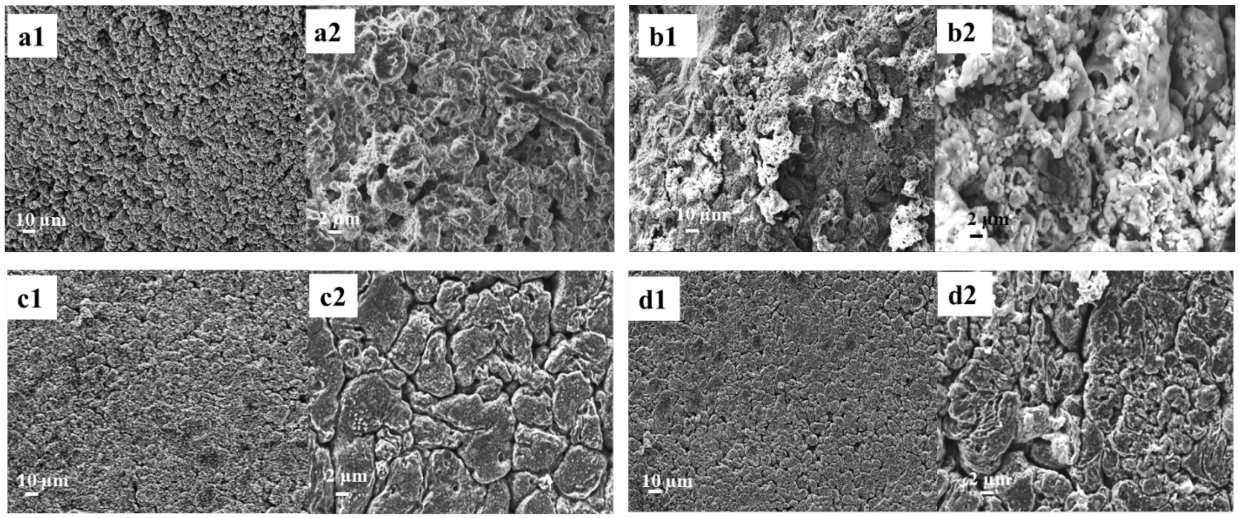

Figure 5. SEM Images of cycled Li- metal anode: with C-2400 after **a1-a2)** 100 and **b1-b2)** 200 cycles; with PDA@BC after **c1-c2)** 100 cycles and **d1-d2)** 500 cycles.

Hence, PDA@BC membrane can be successfully implemented in a Li-S battery to stop the PS shuttling. However, with repeated cycling there is expected degradation in the Li-S battery caused by the repeated SEI formation and its ultimate protrusions through the separators [75]. The effect of this degradation on the separator is studied with the help of a split cell. A Li-S cell with PDA@BC is assembled and disassembled inside a glove box after 0, 50, 100 and finally 350 cycles to study this physical degradation in the separator. This battery was run at 1C and after each assembly it was run at 0.1C for few cycles to facilitate SEI formation. Fig. 6 a and b show the specific capacity of each cycle span and its corresponding optical image of the separator which was taken after disassembly and washing of separator with DME at the end of the cycle span. The blackish color of the separator slightly fades after 100 cycles, with the appearance of several spots on the final separator. Since the black component is PDA, the stress generated in the cycling may degrade the PDA@BC separator by PDA partially peeling off. It is clear from the figure that with more cycles, the separator lost more PDA until the cell finally failed. Therefore, addressing the stability of PDA@BC shall further improve the Li-S battery performance when this novel PDA@BC separator is used.

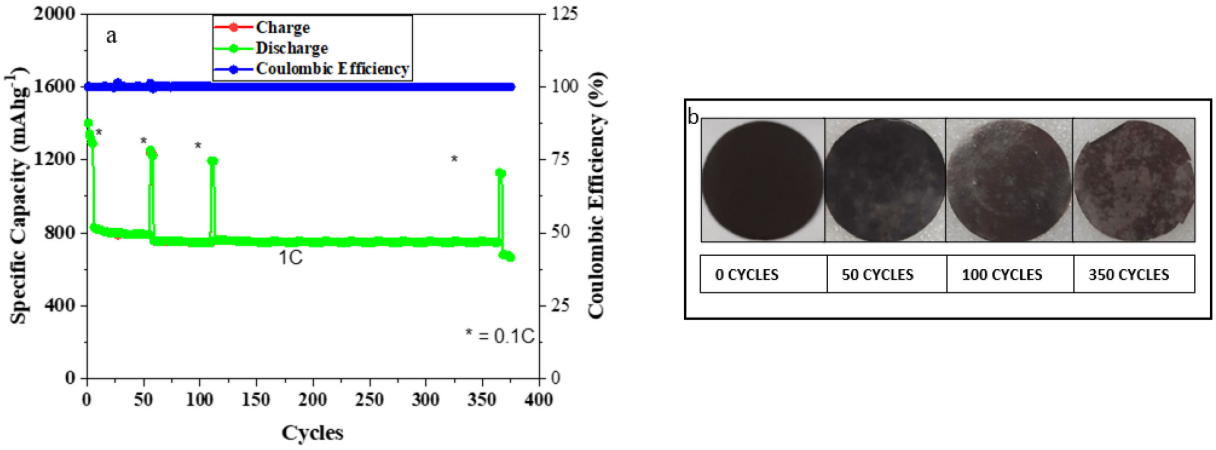

Figure 6. a) Li-S battery performance at 1C with PDA@BC separator (dissembled at specified cycles in b**.** After each disassembly they were run at 0.1C for 3 cycles) **b)** Optical images of PDA@BC separator showing degradation after specified number of cycles.

Conclusion

In previous studies, bacterial cellulose (BC) membranes were utilized as separators in Li-S batteries, yielding a capacity of around 600 mAh g^{-1} at a rate of 0.2 C after 200 charge-discharge cycles[76], considerably lower than sulfur's theoretical capacity. To address this limitation, we combined BC with polydopamine (PDA) to create a 30 µm thick separator. This innovative approach effectively tackled issues related to polysulfide shuttling and dendrite formation in Li-S batteries. The PDA-functionalized BC membranes provided active sites for chemical entrapment of polysulfides, preventing their migration to the anode. Once trapped, an electrostatic effect hindered further polysulfide diffusion. Additionally, some functional groups in PDA@BC facilitated Li^+ ion migration, enhancing cation transference numbers. Moreover, the uniform porous structure of PDA@BC ensured even Li^+ ion flux at the Li-metal anode, preventing localized high flux density. This uniformity facilitated the consistent deposition and removal of lithium, suppressing dendrite formation. These advancements led to Li-S batteries using the innovative PDA@BC separator achieving a remarkable capacity of 1449 mAh g^{-1} at 0.1C, with only 0.03% average

decay per cycle at 1 C over 650 cycles. This outstanding performance was maintained even under high sulfur loading conditions (5 mg cm^{-2}).

Due to its superior conductivity, transference number, wettability, and thermal resistance, PDA@BC holds promise for practical Li-S batteries. Additionally, its applicability can be extended to sodium-sulfur and potassium-sulfur electrochemistry.

Acknowledgment

This research was funded by National Science Foundation of U.S.A, grant number 2103582 and 2129983. We acknowledge the use of facilities within the Eyring Materials Center at Arizona State University, supported in part by NNCI-ECCS-2025490.

References

1. Peng, L.; Wei, Z.; Wan, C.; Li, J.; Chen, Z.; Zhu, D.; Baumann, D.; Liu, H.; Allen, C. S.; Xu, X., A fundamental look at electrocatalytic sulfur reduction reaction. *Nature Catalysis* **2020,** *3* (9), 762-770.
2. Li, S.; Fan, Z., Encapsulation methods of sulfur particles for lithium-sulfur batteries: A review. *Energy Storage Materials* **2021,** *34*, 107-127.
3. Li, S.; Zhang, W.; Zheng, J.; Lv, M.; Song, H.; Du, L., Inhibition of polysulfide shuttles in Li–S batteries: modified separators and solid-state electrolytes. *Advanced Energy Materials* **2021,** *11* (2), 2000779.
4. Weng, Y.-T.; Wang, H.; Lee, R.-C.; Huang, C.-Y.; Huang, S.-S.; Abdollahifar, M.; Kuo, L.-M.; Hwang, B.-J.; Kuo, C.-L.; Cui, Y., Efficient synthesis of high-sulfur-content cathodes for high-performance Li–S batteries based on solvothermal polysulfide chemistry. *Journal of Power Sources* **2020,** *450*, 227676.
5. Li, S.; Leng, D.; Li, W.; Qie, L.; Dong, Z.; Cheng, Z.; Fan, Z., Recent progress in developing Li2S cathodes for Li–S batteries. *Energy Storage Materials* **2020,** *27*, 279-296.
6. Tao, X.; Wang, J.; Liu, C.; Wang, H.; Yao, H.; Zheng, G.; Seh, Z. W.; Cai, Q.; Li, W.; Zhou, G., Balancing surface adsorption and diffusion of lithium-polysulfides on nonconductive oxides for lithium–sulfur battery design. *Nature communications* **2016,** *7* (1), 1-9.
7. Wang, L.; Song, Y.-H.; Zhang, B.-H.; Liu, Y.-T.; Wang, Z.-Y.; Li, G.-R.; Liu, S.; Gao, X.-P.; interfaces, Spherical metal oxides with high tap density as sulfur host to enhance cathode volumetric capacity for lithium–sulfur battery. *ACS applied materials* **2020,** *12* (5), 5909-5919.
8. Zhang, C.; He, Y.; Wang, Y.; Liang, Y.; Majeed, A.; Yang, Z.; Yao, S.; Shen, X.; Li, T.; Qin, S., CoFe2O4 nanoparticles loaded N-doped carbon nanofibers networks as electrocatalyst for enhancing redox kinetics in Li-S batteries. *Applied Surface Science* **2021,** *560*, 149908.
9. Yao, S.; Bi, M.; Yu, H.; Zhang, C.; Zhang, X.; Liu, H.; Zhang, T.; Xiang, J.; Shen, X., Spinel manganese-cobalt oxide nanospheres anchored on nitrogen-containing carbon nanofibers as a highly efficient redox electrocatalyst in lithium/polysulfides batteries. *Applied Surface Science* **2022,** *598*, 153787.

10. Yao, S.; He, Y.; Wang, Y.; Bi, M.; Liang, Y.; Majeed, A.; Yang, Z.; Shen, X., Porous N-doped carbon nanofibers assembled with nickel ferrite nanoparticles as efficient chemical anchors and polysulfide conversion catalyst for lithium-sulfur batteries. *Journal of Colloid and Interface Science* **2021,** *601*, 209-219.
11. Yao, S.; Zhang, C.; Xie, F.; Xue, S.; Gao, K.; Guo, R.; Shen, X.; Li, T.; Qin, S., Hybrid membrane with SnS2 nanoplates decorated nitrogen-doped carbon nanofibers as binder-free electrodes with ultrahigh sulfur loading for lithium sulfur batteries. *ACS Sustainable Chemistry & Engineering* **2020,** *8* (7), 2707-2715.
12. Lu, C.; Chen, Y.; Yang, Y.; Chen, X., Single-atom catalytic materials for lean-electrolyte ultrastable lithium–sulfur batteries. *Nano Letters* **2020,** *20* (7), 5522-5530.
13. Zhang, S.; Ao, X.; Huang, J.; Wei, B.; Zhai, Y.; Zhai, D.; Deng, W.; Su, C.; Wang, D.; Li, Y., Isolated Single-Atom Ni–N5 Catalytic Site in Hollow Porous Carbon Capsules for Efficient Lithium–Sulfur Batteries. *Nano Letters* **2021,** *21* (22), 9691-9698.
14. Zhuang, Z.; Kang, Q.; Wang, D.; Li, Y., Single-atom catalysis enables long-life, high-energy lithium-sulfur batteries. *Nano Letters* **2020,** *13* (7), 1856-1866.
15. Lin, X.; Li, W.; Nguyen, V.; Wang, S.; Yang, S.; Ma, L.; Du, Y.; Wang, B.; Fan, Z., Fe-single-atom catalyst nanocages linked by bacterial cellulose-derived carbon nanofiber aerogel for Li-S batteries. *Chemical Engineering Journal* **2023**, 146977.
16. Li, S.; Mou, T.; Ren, G.; Warzywoda, J.; Wei, Z.; Wang, B.; Fan, Z., Gel based sulfur cathodes with a high sulfur content and large mass loading for high-performance lithium–sulfur batteries. *Journal of Materials Chemistry A* **2017,** *5* (4), 1650-1657.
17. Luo, M.; Bai, Y.; Sun, R.; Qu, M.; Wang, M.; Yang, Z.; Wang, Z.; Sun, W.; Sun, K., Enhancing anchoring and catalytic conversion of polysulfides by nitrogen deficient cobalt nitride for advanced lithium-sulfur batteries. *Journal of Energy Chemistry* **2022,** *73*, 407-415.
18. He, Y.; Qiao, Y.; Zhou, H., Recent advances in functional modification of separators in lithium–sulfur batteries. *Dalton Transactions* **2018,** *47* (20), 6881-6887.
19. Fu, Y.; Wu, Z.; Yuan, Y.; Chen, P.; Yu, L.; Yuan, L.; Han, Q.; Lan, Y.; Bai, W.; Kan, E., Switchable encapsulation of polysulfides in the transition between sulfur and lithium sulfide. *Nature Communications* **2020,** *11* (1), 845.
20. Li, Y.; Zhou, P.; Li, H.; Gao, T.; Zhou, L.; Zhang, Y.; Xiao, N.; Xia, Z.; Wang, L.; Zhang, Q., A freestanding flexible single-atom cobalt-based multifunctional interlayer toward reversible and durable lithium-sulfur batteries. *Small Methods* **2020,** *4* (3), 1900701.
21. Dai, X.; Wang, X.; Lv, G.; Wu, Z.; Liu, Y.; Sun, J.; Liu, Y.; Chen, Y., Defect-engineered Sulfur Vacancy Modified NiCo2S4-x Nanosheet Anchoring Polysulfide for Improved Lithium Sulfur Batteries. *Small* **2023**, 2302267.
22. Dai, X.; Lv, G.; Wu, Z.; Wang, X.; Liu, Y.; Sun, J.; Wang, Q.; Xiong, X.; Liu, Y.; Zhang, C., Flexible Hierarchical Co-Doped NiS2@ CNF-CNT Electron Deficient Interlayer with Grass-Roots Structure for Li–S Batteries. *Advanced Energy Materials* **2023**, 2300452.
23. Dai, X.; Zou, K.; Jing, W.; Xu, P.; Sun, J.; Guo, S.; Tan, Q.; Liu, Y.; Zhou, T.; Chen, Y., A dual-functional interlayer for Li–S batteries using carbon fiber film cladded electron-deficient Li 2 B 4 O 7. *Journal of Materials Chemistry A* **2022,** *10* (30), 16152-16162.
24. Yu, B.; Fan, Y.; Mateti, S.; Kim, D.; Zhao, C.; Lu, S.; Liu, X.; Rong, Q.; Tao, T.; Tanwar, K. K., An Ultra-Long-Life Flexible Lithium–Sulfur Battery with Lithium Cloth Anode and Polysulfone-Functionalized Separator. *ACS nano* **2020,** *15* (1), 1358-1369.
25. Liu, H.; Lai, W.-H.; Yang, H.-L.; Zhu, Y.-F.; Lei, Y.-J.; Zhao, L.; Peng, J.; Wang, Y.-X.; Chou, S.-L.; Liu, H.-K., Efficient separators with fast Li-ion transfer and high polysulfide entrapment for superior lithium-sulfur batteries. *Chemical Engineering Journal* **2021,** *408*, 127348.

26. Li, Q.; Liu, Y.; Yang, L.; Wang, Y.; Liu, Y.; Chen, Y.; Guo, X.; Wu, Z.; Zhong, B., N, O co-doped chlorella-based biomass carbon modified separator for lithium-sulfur battery with high capacity and long cycle performance. *Journal of Colloid and Interface Science* **2021,** *585*, 43-50.
27. Xiao, R.; Yang, S.; Yu, T.; Hu, T.; Zhang, X.; Xu, R.; Wang, Y.; Guo, X.; Sun, Z.; Li, F., A Janus Separator for Inhibiting Shuttle Effect and Lithium Dendrite in Lithium− Sulfur Batteries. *Batteries Supercaps* **2022,** *5* (4), e202100389.
28. Wei, Z.; Zhang, N.; Feng, T.; Wu, F.; Zhao, T.; Chen, R., A copolymer microspheres-coated separator to enhance thermal stability of lithium-sulfur batteries. *Chemical Engineering Journal* **2022,** *430*, 132678.
29. Jing, W.; Zu, J.; Zou, K.; Dai, X.; Song, Y.; Han, J.; Sun, J.; Tan, Q.; Chen, Y.; Liu, Y., Sandwich-like strontium fluoride graphene-modified separator inhibits polysulfide shuttling and lithium dendrite growth in lithium–sulfur batteries. *Journal of Materials Chemistry A* **2022,** *10* (9), 4833-4844.
30. Zhang, K.; Chen, Z.; Ning, R.; Xi, S.; Tang, W.; Du, Y.; Liu, C.; Ren, Z.; Chi, X.; Bai, M., Single-atom coated separator for robust lithium–sulfur batteries. *ACS applied materials interfaces* **2019,** *11* (28), 25147-25154.
31. Hong, X.-J.; Song, C.-L.; Yang, Y.; Tan, H.-C.; Li, G.-H.; Cai, Y.-P.; Wang, H., Cerium based metal–organic frameworks as an efficient separator coating catalyzing the conversion of polysulfides for high performance lithium–sulfur batteries. *ACS nano* **2019,** *13* (2), 1923-1931.
32. Lin, G.; Jia, K.; Bai, Z.; Liu, C.; Liu, S.; Huang, Y.; Liu, X., Metal-Organic Framework Sandwiching Porous Super-Engineering Polymeric Membranes as Anionphilic Separators for Dendrite-free Lithium Metal Batteries. *Advanced Functional Materials* **2022,** *32* (47), 2207969.
33. Mathew, D. E.; Gopi, S.; Kathiresan, M.; Rani, G. J.; Thomas, S.; Stephan, A. M., A porous organic polymer-coated permselective separator mitigating self-discharge of lithium–sulfur batteries. *Materials Advances* **2020,** *1* (4), 648-657.
34. Wu, X.; Fan, L.; Qiu, Y.; Wang, M.; Cheng, J.; Guan, B.; Guo, Z.; Zhang, N.; Sun, K., Ion-Selective Prussian-Blue-Modified Celgard Separator for High-Performance Lithium–Sulfur Battery. *ChemSusChem* **2018,** *11* (18), 3345-3351.
35. Wang, J.; Zhu, Y.; Wu, N.; Kan, Y.; Hu, Y., Designing thermotolerant and flame-resistant PAN-based separator via surface engineering with heteroatoms doped carbon framework encapsulated with CoS2 nanocatalysts towards safe lithium-sulfur batteries. *Composites Part B: Engineering* **2022,** *233*, 109644.
36. Jiang, F.; Yin, L.; Yu, Q.; Zhong, C.; Zhang, J., Bacterial cellulose nanofibrous membrane as thermal stable separator for lithium-ion batteries. *Journal of Power Sources* **2015,** *279*, 21-27.
37. Li, M.; Wang, X.; Yang, Y.; Chang, Z.; Wu, Y.; Holze, R., A dense cellulose-based membrane as a renewable host for gel polymer electrolyte of lithium ion batteries. *Journal of membrane science* **2015,** *476*, 112-118.
38. Li, W.; Wang, S.; Fan, Z.; Li, S.; Newman, N., Oxidized bacterial cellulose functionalized with SiO2 nanoparticles as a separator for lithium-metal and lithium–sulfur batteries. *Cellulose* **2022**, 1-13.
39. Zhang, T.; Yang, L.; Yan, X.; Ding, X., Recent advances of cellulose-based materials and their promising application in sodium-ion batteries and capacitors. *Small* **2018,** *14* (47), 1802444.
40. Zhou, W.; Chen, M.; Tian, Q.; Chen, J.; Xu, X.; Wong, C.-P., Cotton-derived cellulose film as a dendrite-inhibiting separator to stabilize the zinc metal anode of aqueous zinc ion batteries. *Energy Storage Materials* **2022,** *44*, 57-65.
41. Li, J.; Klöpsch, R.; Nowak, S.; Kunze, M.; Winter, M.; Passerini, S., Investigations on cellulose-based high voltage composite cathodes for lithium ion batteries. *Journal of Power Sources* **2011,** *196* (18), 7687-7691.

42. Li, W.; Wang, S.; Fan, Z.; Li, S.; Bernussi, A.; Newman, N., Functionalized bacterial cellulose as a separator to address polysulfides shuttling in lithium–sulfur batteries. *Materials Today Energy* **2021,** *21*, 100813.
43. Liu, J.; Wang, D.; Zhang, D.; Gao, L.; Lin, T., Synergistic effects of carboxymethyl cellulose and ZnO as alkaline electrolyte additives for aluminium anodes with a view towards Al-air batteries. *Journal of Power Sources* **2016,** *335*, 1-11.
44. Cheng, M.; Liu, J.; Wang, X.; Li, Y.; Xia, W.; Liu, Q.; Hu, J.; Wei, T.; Ling, Y.; Liu, B., In-situ synthesis of Bi nanospheres anchored in 3D interconnected cellulose nanocrystal derived carbon aerogel as anode for high-performance Mg-ion batteries. *Chemical Engineering Journal* **2023,** *451*, 138824.
45. Ma, L.; Bi, Z.; Xue, Y.; Zhang, W.; Huang, Q.; Zhang, L.; Huang, Y., Bacterial cellulose: an encouraging eco-friendly nano-candidate for energy storage and energy conversion. *Journal of Materials Chemistry A* **2020,** *8* (12), 5812-5842.
46. Huang, Q.; Chen, J.; Liu, M.; Huang, H.; Zhang, X.; Wei, Y., Polydopamine-based functional materials and their applications in energy, environmental, and catalytic fields: State-of-the-art review. *Chemical Engineering Journal* **2020,** *387*, 124019.
47. Delparastan, P.; Malollari, K. G.; Lee, H.; Messersmith, P. B., Direct evidence for the polymeric nature of polydopamine. *Angewandte Chemie* **2019,** *131* (4), 1089-1094.
48. Zhou, W.; Xiao, X.; Cai, M.; Yang, L., Polydopamine-coated, nitrogen-doped, hollow carbon–sulfur double-layered core–shell structure for improving lithium–sulfur batteries. *Nano letters* **2014,** *14* (9), 5250-5256.
49. Xu, Q.; Kong, Q.; Liu, Z.; Zhang, J.; Wang, X.; Liu, R.; Yue, L.; Cui, G., Polydopamine-coated cellulose microfibrillated membrane as high performance lithium-ion battery separator. *Rsc Advances* **2014,** *4* (16), 7845-7850.
50. Szabó, L. s.; Imanishi, S.; Hirose, D.; Tsukegi, T.; Wada, N.; Takahashi, K., Mussel-inspired design of a carbon fiber–cellulosic polymer interface toward engineered biobased carbon fiber-reinforced composites. *ACS omega* **2020,** *5* (42), 27072-27082.
51. Hemmatpour, H.; De Luca, O.; Crestani, D.; Stuart, M. C.; Lasorsa, A.; van der Wel, P. C.; Loos, K.; Giousis, T.; Haddadi-Asl, V.; Rudolf, P., New insights in polydopamine formation via surface adsorption. *Nature Communications* **2023,** *14* (1), 664.
52. Zhang, J.; Yue, L.; Kong, Q.; Liu, Z.; Zhou, X.; Zhang, C.; Xu, Q.; Zhang, B.; Ding, G.; Qin, B., Sustainable, heat-resistant and flame-retardant cellulose-based composite separator for high-performance lithium ion battery. *Scientific reports* **2014,** *4* (1), 1-8.
53. Chun, S.-J.; Choi, E.-S.; Lee, E.-H.; Kim, J. H.; Lee, S.-Y.; Lee, S.-Y., Eco-friendly cellulose nanofiber paper-derived separator membranes featuring tunable nanoporous network channels for lithium-ion batteries. *Journal of Materials Chemistry A* **2012,** *22* (32), 16618-16626.
54. Dumitriu, C.; Voicu, S. I.; Muhulet, A.; Nechifor, G.; Popescu, S.; Ungureanu, C.; Carja, A.; Miculescu, F.; Trusca, R.; Pirvu, C., Production and characterization of cellulose acetate–titanium dioxide nanotubes membrane fraxiparinized through polydopamine for clinical applications. *Carbohydrate polymers* **2018,** *181*, 215-223.
55. Liu, X.; Wu, Y.; Lin, Q.; Cheng, J.; Lin, F.; Tang, L.; Huang, B.; Lu, B., Polydopamine-coated cellulose nanocrystal as functional filler to fabricate nanocomposite hydrogel with controllable performance in response to near-infrared light. *Cellulose* **2021,** *28*, 2255-2271.
56. Li, S.; Warzywoda, J.; Wang, S.; Ren, G.; Fan, Z., Bacterial cellulose derived carbon nanofiber aerogel with lithium polysulfide catholyte for lithium–sulfur batteries. *Carbon* **2017,** *124*, 212-218.
57. Ball, V.; Del Frari, D.; Toniazzo, V.; Ruch, D., Kinetics of polydopamine film deposition as a function of pH and dopamine concentration: Insights in the polydopamine deposition mechanism. *Journal of colloid interface science* **2012,** *386* (1), 366-372.

58. Sun, J.; Hwang, J. Y.; Jankowski, P.; Xiao, L.; Sanchez, J. S.; Xia, Z.; Lee, S.; Talyzin, A. V.; Matic, A.; Palermo, V., Critical role of functional groups containing N, S, and O on graphene surface for stable and fast charging Li-S batteries. *Small* **2021,** *17* (17), 2007242.
59. Francis, C. F.; Kyratzis, I. L.; Best, A. S., Lithium-ion battery separators for ionic-liquid electrolytes: a review. *Advanced Materials Interfaces* **2020,** *32* (18), 1904205.
60. Jiang, W.; Yang, X.; Deng, J.; Zhang, J.; Zhang, G., Polydopamine-based materials applied in Li-ion batteries: a review. *Journal of Materials Science* **2021**, 1-24.
61. Sun, T.; Li, Z. j.; Wang, H. g.; Bao, D.; Meng, F. l.; Zhang, X. b., A biodegradable polydopamine-derived electrode material for high-capacity and long-life lithium-ion and sodium-ion batteries. *Angewandte Chemie International Edition* **2016,** *55* (36), 10662-10666.
62. Liebscher, J. r.; Mrówczyński, R.; Scheidt, H. A.; Filip, C.; Hădade, N. D.; Turcu, R.; Bende, A.; Beck, S., Structure of polydopamine: a never-ending story? *Langmuir* **2013,** *29* (33), 10539-10548.
63. Liu, B.; Torres, J. F.; Taheri, M.; Xiong, P.; Lu, T.; Zhu, J.; Liu, Y.; Yu, G.; Tricoli, A., Dual-Ion Flux Management for Stable High Areal Capacity Lithium–Sulfur Batteries. *Advanced Energy Materials* **2022,** *12* (10), 2103444.
64. Zhu, X.; Zhao, W.; Song, Y.; Li, Q.; Ding, F.; Sun, J.; Zhang, L.; Liu, Z., In situ assembly of 2D conductive vanadium disulfide with graphene as a high-sulfur-loading host for lithium–Sulfur batteries. *Advanced Energy Materials* **2018,** *8* (20), 1800201.
65. Zhou, M.-L.; Zhang, Z.; Xu, J.; Wei, J.; Yu, J.; Yang, Z.-Y., PDA modified commercial paper separator engineering with excellent lithiophilicity and mechanical strength for lithium metal batteries. *Journal of Electroanalytical Chemistry* **2020,** *868*, 114195.
66. Tian, Y.; Sun, Z.; Zhang, Y.; Wang, X.; Bakenov, Z.; Yin, F., Micro-spherical sulfur/graphene oxide composite via spray drying for high performance lithium sulfur batteries. *Nanomaterials* **2018,** *8* (1), 50.
67. Zhou, G., Graphene–pure sulfur sandwich structure for ultrafast, long-life lithium-sulfur batteries. In *Design, Fabrication and Electrochemical Performance of Nanostructured Carbon Based Materials for High-Energy Lithium–Sulfur Batteries*, Springer: 2017; pp 75-94.
68. Um, J. H.; Yu, S. H., Unraveling the mechanisms of lithium metal plating/stripping via in situ/operando analytical techniques. *Advanced Energy Materials* **2021,** *11* (27), 2003004.
69. Zheng, J.; Tian, J.; Wu, D.; Gu, M.; Xu, W.; Wang, C.; Gao, F.; Engelhard, M. H.; Zhang, J.-G.; Liu, J., Lewis acid–base interactions between polysulfides and metal organic framework in lithium sulfur batteries. *Nano letters* **2014,** *14* (5), 2345-2352.
70. Yang, Y.; Wang, W.; Li, L.; Li, B.; Zhang, J., Stable cycling of Li–S batteries by simultaneously suppressing Li-dendrite growth and polysulfide shuttling enabled by a bioinspired separator. *Journal of Materials Chemistry A* **2020,** *8* (7), 3692-3700.
71. Yang, Y.; Zhang, J., Highly Stable Lithium–Sulfur Batteries Based on Laponite Nanosheet-Coated Celgard Separators. *Advanced Energy Materials* **2018,** *8* (25), 1801778.
72. Song, J.; Gordin, M. L.; Xu, T.; Chen, S.; Yu, Z.; Sohn, H.; Lu, J.; Ren, Y.; Duan, Y.; Wang, D., Strong lithium polysulfide chemisorption on electroactive sites of nitrogen-doped carbon composites for high-performance lithium–sulfur battery cathodes. *Angewandte Chemie* **2015,** *127* (14), 4399-4403.
73. Wang, J.; Zhang, J.; Duan, S.; Li, T.; Jia, L.; Liu, H.; Li, L.; Cheng, S.; Hu, H.; Huang, M., Interfacial lithium-nitrogen bond catalyzes sulfide oxidation reactions in high-loading Li2S cathode. *Chemical Engineering Journal* **2022,** *429*, 132352.
74. Knap, V.; Stroe, D.-I.; Swierczynski, M.; Teodorescu, R.; Schaltz, E., Investigation of the self-discharge behavior of lithium-sulfur batteries. *Journal of The Electrochemical Society* **2016,** *163* (6), A911.
75. Harrison, K. L.; Merrill, L. C.; Long, D. M.; Randolph, S. J.; Goriparti, S.; Christian, J.; Warren, B.; Roberts, S. A.; Harris, S. J.; Perry, D. L., Cryogenic electron microscopy reveals that applied pressure promotes short circuits in Li batteries. *Iscience* **2021,** *24* (12), 103394.

76. Zhang, Z.; Li, Y.; Cui, X.; Guan, S.; Tu, L.; Tang, H.; Li, Z.; Li, J., Understanding the Advantageous Features of Bacterial Cellulose-Based Separator in Li–S Battery. *Advanced Materials Interfaces* **2023,** *10* (1), 2201730.